ISSN 1682-296X (Print)
ISSN 1682-2978 (Online)

Bio Technology

ANSInet
Asian Network for Scientific Information
308 Lasani Town, Sargodha Road, Faisalabad - Pakistan

Biotechnology 6 (2): 153-164, 2007
ISSN 1682-296X

Design of Wireless Power and Data Transmission Circuits for Implantable Biomicrosystem

Ghazi Ben Hmida, Hamadi Ghariani and Mounir Samet
Laboratory of Electronics and Technology of Information (LETI), Department of Electrical Engineering, National Engineers School of Sfax, B.P. W, Sfax, Tunisia 3038, Tunisia

Abstract: This study describes the design of an inductive powering system that combines power transfer with data transmission for implantable biomicrosystem. The implant receives power from an external transmitter through an inductive link between an external power transmission coil and the implanted receiving coil. We designed a transmitter with class E power amplifier to provide maximum power with high-efficiency. It is possible to obtain about 136 mW of power in the secondary system with an efficiency of about 50%. A bit rate of 1 Mbps is achieved for sending command data to the implant. We propose a communication system for the medical implants which uses inductive link. This system is consisted of a class E power amplifier, an ASK modulator, an inductive link and an ASK demodulator.

Key words: Biomicrosystem, power-data transfer, inductive link, class E amplifier

INTRODUCTION

Implantable stimulators such as pacemakers, defibrillators, cochlear implants, instrumented orthopaedic implants, deep brain and spinal cord stimulators have found a variety of applications in improving the quality of patient's lives (Pamela *et al*., 2006; Burny *et al*., 2000, Loeb *et al*., 1998; Wise *et al*., 2004). Broad research is underway to provide new devices for other applications such as visual prosthesis, recording devices and neuromuscular controllers (Margalit *et al*., 2002; Stangel *et al*., 2001; Mohseni and Najafi, 2005; Harrison *et al*., 2007; Harrison and Charles, 2003; Watkins *et al*., 2006; Sawan, 2004). Reducing the size and power consumption have been the two major challenges in designing these implantable microelectronics because the implantation procedure should be minimally invasive to the patient. Batteries are not the optimal choice for implantable devices, because their lifetime is limited and they are usually large and leaks can pose a hazard to tissues. For most of these long-term implantable devices, an external transcutaneous wireless link is preferred to an internal battery for the power supply (Galbraith, 1987; Catrysse *et al*., 2004). Wireless operation is required for most of the biomedical implantable circuits. Many of these devices are powered by inductive coupling in the centimetre range distance over the skin barrier. Some of the biomedical implants, particularly those which interface with the central nervous system, such as cochlear and visual prostheses, need large amounts of data to simultaneously interface with a large number of neurons through multiple channels (Suaning and Lovell, 2001; Wang *et al*., 2004). Therefore, a high data-rate receiver circuitry that can establish an efficient wireless link between the implant and the external units is highly needed.

Present study field is interested to the cochlear implant (Ghorbel *et al*., 2006) and implanted micro-sensor system for measurements and recording of neural signal from auditory nerve. The main objective of this study is to supply medical implant with power and data. In this study, we present inductive powering system that has been optimised towards maximal power transfer efficiency and high data rate. The crucial point of this study is to achieve a power efficiency of 50% and 1 Mbit sec^{-1} data rate.

Figure 1 shows the synoptic diagram of wireless powering and data communication for implantable

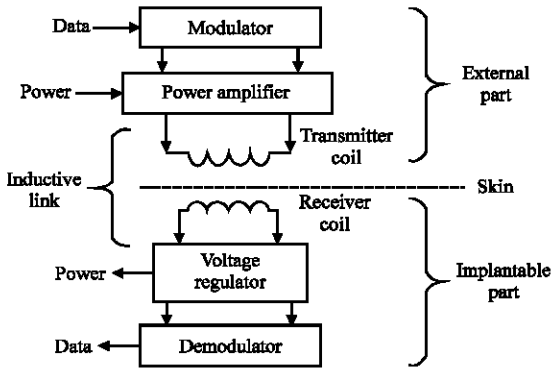

Fig. 1: Block diagram of wireless biomedical implex communication

Corresponding Author: Ghazi Ben Hmida, Laboratory of Electronics and Technology of Information (LETI), Department of Electrical Engineering, National Engineers School of Sfax, B.P. W, Sfax, Tunisia 3038, Tunisia

medical devices. The external part is consisting of a modulator and power amplifier. The internal part contains voltage regulator and demodulator. Then, the implanted device is externally controlled and powered by a modulated radio frequency signal. The receiver circuitry of the implant provides the stably regulated voltage and demodulates the data from radio frequency signal (Ben Hmida *et al*., 2006).

INDUCTIVE LINK

An inductive link, when used in implanted biomedical instruments, is also known as a transcutaneous transformer, since its primary and secondary coils are physically separated and communicate through the electromagnetic field linking the two coils. Extensive research has been performed to analyze and optimize the operation of such inductive links (Gervais *et al*., 2003) and there exist many applications of inductive links to deliver power and data into implants (Huang and Oberle, 1998).

Equivalent electrical circuit: The equivalent electrical circuit of an inductive link is depicted in Fig. 2. It consists of the self-inductances L_n and resistances R_{Ln} of the primary and secondary coil (where n = 1, 2), the mutual inductance M between the two coils, the link load impedance Z_2 and a voltage source V_1. The equivalent circuit can be described by Eq. 1 through Eq. 3.

$$V_1 = j\omega L_1 I_1 + R_{L1} I_1 + j\omega M I_2 \quad (1)$$

$$V_2 = j\omega M L_1 I_1 + j\omega L_2 I_2 R_{L2} I_2 \quad (2)$$

$$V_2 = -Z_2 I_2 \quad (3)$$

An often used measure for the coupling between two coils is the coupling factor or coupling coefficient k, given by:

$$k = \frac{M}{\sqrt{L_1 L_2}} \quad (4)$$

Physically, the coupling factor equals the fraction of magnetic flux generated by the primary coil L_1, which flows through the secondary coil L_2 and as mutual inductance is a reciprocal property of two coils, vice versa. The secondary current I_2 and voltage V_2 can be easily calculated from Eq. 1 through Eq. 3:

$$I_2 = -\frac{j\omega M}{j\omega L_2 + R_{L2} + Z_2} I_1 \quad (5)$$

$$\frac{V_2}{V_1} = \frac{j\omega M Z_2}{\omega^2 (M^2 - L_1 L_2) + j\omega (L_1 Z_2 + L_1 R_{L2} + L_2 R_{L1}) + R_{L1} Z_2 + R_{L1} R_{L2}} \quad (6)$$

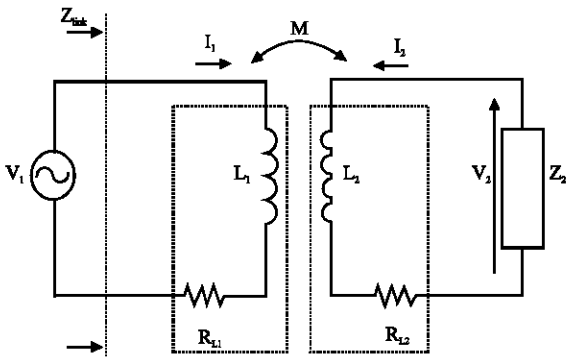

Fig. 2: Schematic overview of an inductive link

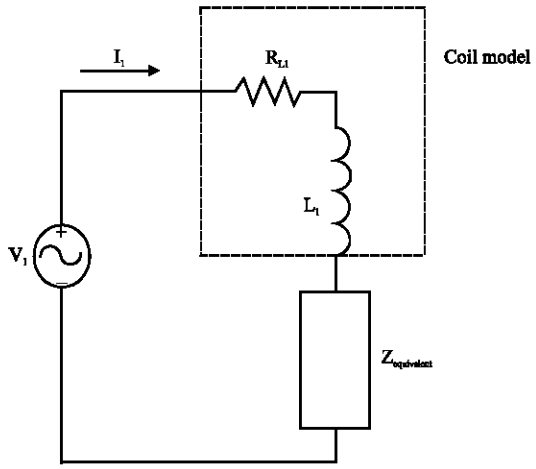

Fig. 3: Equivalent circuit of inductive link transformed into Zequivalent

The link impedance Z_{link} as seen from the voltage source V_1 in Fig. 2 is also easily calculated from the link equations and is given by:

$$Z_{Link} = \frac{V_1}{I_1} = j\omega L_1 + R_{L1} + Z_{equivalent} \quad (7)$$

in which $Z_{equivalent}$ is the equivalent impedance of the secondary circuit as seen by the primary circuit, as shown in Fig. 3:

The expression of the equivalent impedance is given by:

$$Z_{equivalent} = \frac{\omega^2 M^2}{j\omega L_2 + R_{L2} + Z_2} \quad (8)$$

The link efficiency η_{link} is defined by the ratio of the power dissipated in the link load impedance Z_2 and the power delivered by the voltage source V_1. It is given by:

$$\eta_{link} = \frac{\Re\acute{e}el\left(V_2 I_2^*\right)}{\Re\acute{e}el\left(V_1 I_1^*\right)} \quad (9)$$

$$\eta_{link} = \frac{\omega^2 M^2 R_2}{R_{L_1}\left(\left(R_{L2}+R_2\right)^2+\left(\omega L_2+X_2\right)^2\right) + \omega^2 M^2\left(R_{L2}+R_2\right)} \quad (10)$$

in which I_n^* is the complex conjugate of I_n and $Z_2 = R_2 + jX_2$.

Optimization and design choices: It can easily be seen from Eq. 10 that the link efficiency η_{link} is maximal when $\omega L_2 = -X_2$. This can be achieved by tuning the secondary coil with a parallel or series capacitance.

Secondary circuit in series resonance: For a series tuned secondary coil as shown in Fig. 4a, the link load resistance R_2 and the link load reactance X_2 become

$$R_2 = R_{load} \quad (11)$$

$$X_2 = -\frac{1}{\omega C_{2s}} \quad (12)$$

where R_{load} is the impedance of the load circuit and C_{2s} is the series capacitance. The optimal choice for the series capacitor C_{2s} is then:

$$C_{2s} = \frac{1}{\omega^2 L_2} \quad (13)$$

The equivalent impedance $Z_{equivalent}$ of the secondary circuit then simplifies to

$$Z_{equivalent} = R_{equivalent} = \frac{\omega^2 M^2}{R_{L2}+R_{load}} \quad (14)$$

Secondary circuit in parallel resonance: For a parallel tuned secondary coil, depicted in Fig. 4b, R_2 and X_2 are given by:

$$R_2 = \frac{R_{load}}{1+\omega^2 R_{load}^2 C_{2p}^2} \quad (15)$$

$$X_2 = -\frac{\omega R_{load}^2 C_{2p}}{1+\omega^2 R_{load}^2 C_{2p}^2} \quad (16)$$

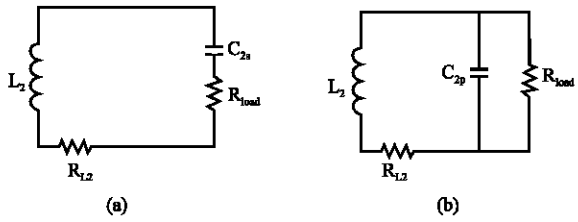

Fig. 4: (a) Series tuned secondary coil and (b) Parallel tuned secondary coil

Table 1: Inductive link parameter values

Operating frequency	f = 13.56 MHZ
Quality factor of the primary coil	$Q_1 = 220$
Quality factor of the secondary coil	$Q_2 = 52$
Primary coil	$L_1 = 5.48\ \mu H$
Secondary coil	$L_2 = 1\ \mu H$
Parasitic resistance of the transmitter coil	$R_{L1} \approx 2.12\ \Omega$
Parasitic resistance of the receiver coil	$R_{L2} \approx 1.63\ \Omega$
Load resistance	$R_{load} = 300\ \Omega$

The optimal choice for the parallel capacitor C_{2p} is:

$$C_{2p} = \frac{R_{load}+\sqrt{R_{load}^2 - 4\omega^2 L_2^2}}{2\omega^2 R_{load} L_2} \quad (17)$$

The equivalent impedance $Z_{equivalent}$ of the secondary circuit then simplifies to

$$Z_{equivalent} = \frac{\omega^2 M^2\left(R_{load}+\sqrt{R_{load}^2 - 4\omega^2 L_2^2}\right)}{2\omega^2 L_2^2 + R_{L2} R_{load} + R_{L2}\sqrt{R_{load}^2 - 4\omega^2 L_2^2}} \quad (18)$$

So that the Eq. 17 and 18 are mathematically true, one must check the following condition:

$$\left(R_{load}^2 - 4\omega^2 L_2^2\right) > 0 \ \Rightarrow\ R_{load} > 2\omega L_2 \quad (19)$$

Application: The model of the inductive link, described earlier, is applied by respecting the requirements of our specifications given by Table 1:

$R_{load} = 300\ \Omega$, which checks the condition given by the Eq. 19, i.e., $R_{load} > 170.4\ \Omega$.

Using software MAPLE, one plots the module of voltage gain curves by using the Eq. 6 and of the link efficiency by using the Eq. 10 versus coupling coefficient k, given respectively by Fig. 5a and b.

One applies the Eq. 6 of the voltage gain for the two cases; series and parallel resonance. By analyzing the curves obtained Fig. 5a, it is noticed that one can achieve a maximum gain of 0.6 for a coupling coefficient about 0.6 for a secondary circuit in parallel resonance. In the case of a series resonance the voltage gain is always lower than that of a parallel tuned secondary circuit.

One applies the Eq. 10 of the link efficiency for the two cases of series and parallel resonance. By analyzing the curves obtained Fig. 5b, it is noticed that one can reach a maximum efficiency about 0.92 for a coupling coefficient higher than 0.2 in the case of a parallel tuned secondary circuit.

The majority of the electronic implants, one uses a coupling coefficient which does not exceed 0.45. In this zone of coupling, the link efficiency given by a secondary circuit tuned in parallel resonance is better than that given by a secondary circuit tuned in series resonance.

Thereafter, we will treat the only case of a parallel resonance since it offers characteristics, such as the voltage gain and the link efficiency, certainly better than that given by a series resonance.

Figures 6a-c give respectively an estimate of the module of voltage gain, link efficiency and the equivalent impedance $Z_{equivalent}$ of the secondary circuit versus the load resistance (275 Ω < R_{load} < 325 Ω) and the coupling coefficient k.

By analyzing the curve given by Fig. 6a, it is noticed that when the load is increased, the voltage gain also increases, for a coupling coefficient lower than 0.6. It is clear that the load variation, between 275 and 325 Ω, does not have a great effect on the gain voltage module. By analyzing the curve given by Fig. 6b, it is observed that when the load is increased, the link efficiency degrades slightly. It is clear that the load variation between 275 and 325 Ω does not have a great effect on the link efficiency. It is also noticed that the link efficiency reaches its maximum for a coupling coefficient higher than 0.3.

The equivalent impedance $Z_{equivalent}$ of the secondary circuit tuned in parallel resonance, given by equation 18, transferred into primary circuit is plotted Fig. 6c. By analyzing this curve; we notice that when the load is increased, the equivalent impedance of the secondary increases slightly. In conclusion, the load variation between 275 and 325 Ω, does not have a great effect, for a given coupling coefficient, on these three preceding characteristics.

By fixing the coefficient of coupling k = 0.1678 (calculated for an average value of the R_{load} = 300 Ω and an equivalent impedance of 39.755Ω), we plotted the curve of the equivalent impedance of the secondary circuit transferred to the primary circuit, gain voltage module and link efficiency versus the load resistance variation Fig. 7a-c.

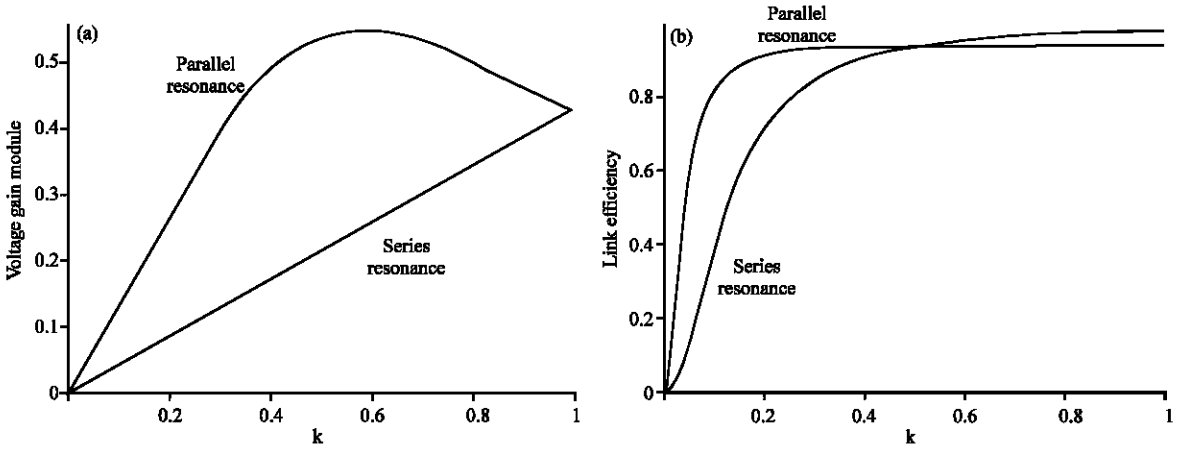

Fig. 5: (a) Voltage gain module and (b) Link efficiency vs coupling coefficient

Fig. 6: (a) Voltage gain module, (b) Link efficiency and (c) Zequivalent, vs load resistance and coupling coefficient

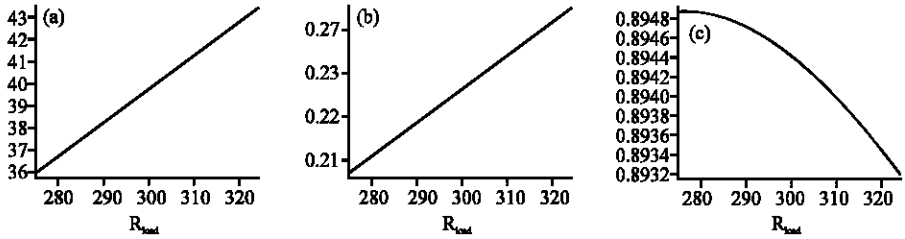

Fig. 7: (a) Equivalent impedance, (b) Gain voltage module and (c) Link efficiency vs resistance

Table 2: Variation of $Z_{equivalent}$, voltage gain and link efficiency for coupling coefficient k = 0.1678

R_{load} (Ω)	275	300	325
$Z_{equivalent}$ (Ω)	35.89	39.75	43.48
Voltage gain	00.206	00.226	00.245
Link efficiency (%)	89.49	89.44	89.31

According to the curve obtained Fig. 7a-b, the equivalent impedance and the gain voltage module follow a linear function in dependence of the load.

Table 2 summarizes the results obtained previously, the coupling coefficient is k = 0.1678.

Inductive link simulation: The electronic circuit of inductive link is depicted in Fig. 8. The primary and the secondary circuit are tuned to the carrier frequency of 13.56 MHZ. By using PSpice simulation, we had plot the gain voltage of the inductive link circuit for some coupling coefficient values (k = 0.01; 0.1; 0.13; 0.15; 0.2; 0.3) at a load of 300 Ω, as shown in Fig. 9. We denote that according to this plot, the inductive link behaves as a pass band filter at the central frequency 13.56 MHZ.

The analysis of this simulation shows that:

- For a coupling coefficient lower than 0.13, the band width is lower than 1 MHZ.
- For a coupling coefficient upper than 0.15, the band width is upper than 1.5 MHZ.

Transmission through biological tissues: The transmission through human tissues is governed by standards. The principal standard fixes a limit for Specific Absorption Rate (SAR). The SAR corresponds to the quantity of power absorbed by biological tissues. Several studies are made to determine the effects of the electromagnetic waves on the human body. It is the case of inductive link which transmits energy through biological tissues.

With an aim of simplifying the analysis, it is appropriate to check initially if one can use the quasi-static approximation. It is the case when the operation distance is negligible compared to the wavelength. For medical implants that use an inductive link, the typical operation distance is nearly 1 cm and the

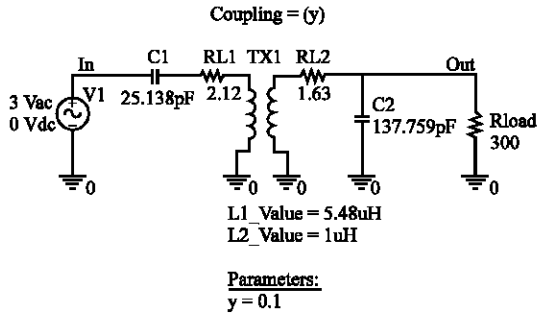

Fig. 8: Electronic circuit of inductive link

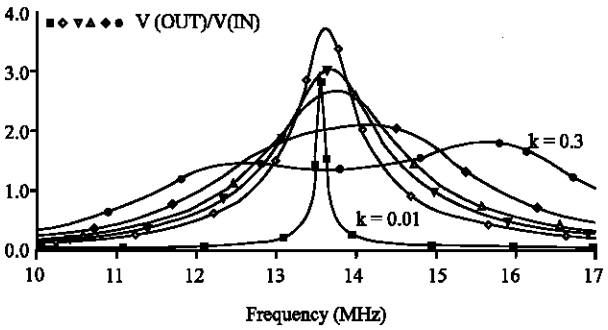

Fig. 9: Voltage gain of inductive link

operating frequency is equal to 13.56 MHZ. In this case, the principal losses of energy will not take place due to the reflections, but by the phenomenon of the Foucault currents. To know the losses, it is necessary to know the conductivity of materials crossed by the magnetic field. The complexity of biological tissues led to several studies, including one very complete made by Gabriel and Gabriel (1996), the results of this study give a mathematical model as well as the various constants for each type of tissues.

The complete analysis of the phenomenon is complicated, but a typical case can be illustrated according to results' presented by Schuder *et al.* (1976). The calculation of power, absorbed by biological tissues (skin), according to the Eq. 20, where K[G] and E[G] are complete elliptic integrals of first and second order, respectively. The other parameters used are provided to Table 3. The evaluation of the Eq. 20 is nearly 0.6 mW.

Table 3: Parameter values used by equation (20)

Symbol	Parameters	Value
I	Current	0.1 A
ω	Angular frequency	85.2 10^6 rad s^{-1}
n	Turns No. of coil	5
μ_0	Permeability of free space	4π 10^{-17} H m^{-1}
a	Radius of transmitter coil	0.0175 m
b	Distance between coil and skin	0.005 m
σ	The conductivity of material	0.23802 S m^{-1}
ρ	Integration variable (radius)	-
z	Integration variable (depth)	-

For a case where the total power exceeds 130 mW, the losses are thus lower than 0.5% and can be regarded as being negligible.

$$P = \frac{I^2\omega^2 n^2 \mu_0^2 a^3 \sigma}{4\pi^2}\int_b^\infty\int_0^\infty\left(\left(\frac{2}{g}-g\right)K[g]-\frac{2}{g}E[g]\right)^2 2\pi d\rho dz \quad (20)$$

With

$$g = \frac{2\rho a^{1/2}}{\left((1+\rho)^2+z^2\right)^{1/2}} \quad (21)$$

CLASS-E POWER AMPLIFIER

The critical element of the external transmitter is the circuit to drive the transmitter coil. There are many types of amplifiers that may be suitable. Among them class D and class-E with both theoretical 100% of efficiency (only ideal switches) are very suitable candidates. The topology chosen is class E. The major advantage of this topology versus other types (like class D or class C) is essentially the easy inclusion of the parasitic drain-source capacitance of the switch transistor into the design optimization.

Circuit analysis: Achieving high power transfer efficiency is one of the challenges that one would face in the design of such systems. For this reason, we use a transmitter with class E power amplifier to provide maximum power transfer with high-efficiency. A structure of class E power amplifier is shown in Fig. 10. A high-speed power switch (MOSFET transistor) drives a resonant network consisting of a parallel capacitor or shunt capacitor (C_d), a transmitter coil (L_1), a tuning capacitor (C) and a resistive load (R_L) i.e., R_L represents the equivalent load of the implanted device with the receiver coil and parasitic resistances of the transmitter coil. When the switch is OFF, the RF choke inductor (RFC) acts as a current source charging the resonant network and creating a transient voltage across the switch. When the switch is ON, its current rises smoothly until the switch is off again (Fig. 11). Losses are kept at minimum by having the transistor switch on when both voltage and current are small (Sokal and Sokal, 1975; Kendir *et al*., 2005). The current and voltage across the transmitter coil are sinusoidal at the resonant frequency of the tank circuit, which has to be the same as the driver switching frequency. The optimum conditions, i.e., Zero-Voltage Switching (ZVS) and Zero-Voltage-derivative Switching (ZVDS) are necessary for the Class E amplifier to achieve high efficiency (Suetsugu and Kazimierczuk, 2004; Raab, 1977; Kazimierczuk and Puczko, 1987). The efficiency of Class E transmitter can reach 100% with theoretical design.

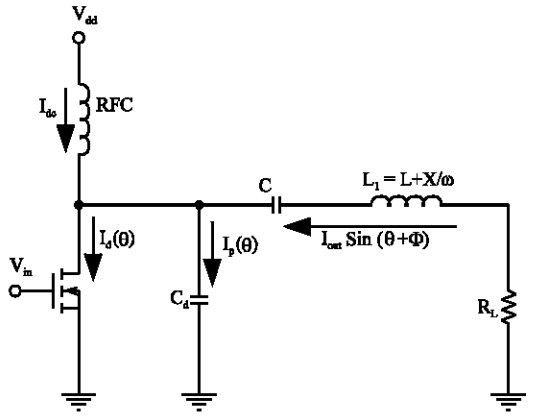

Fig. 10: Basic circuit of the class E amplifier

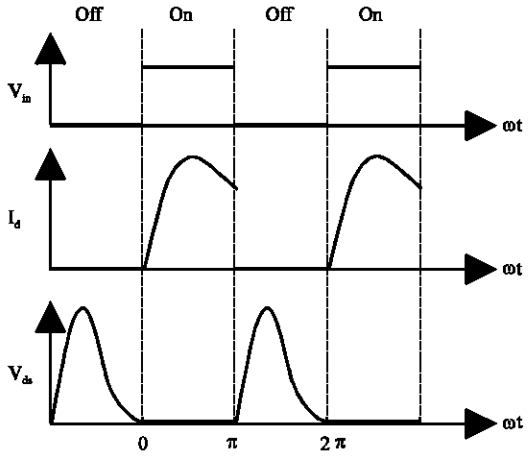

Fig. 11: Theoretical wavesforms of the switch voltage (Vds) and current (Id)

Design of the Analytical Equations for Optimum Operation: The derivations of design equations are carried out under the following assumptions.

- The shunt capacitance of the amplifier consists of the MOSFET output capacitance and an external linear capacitance.
- The inductance of the choke coil is large enough to neglect its current ripple.
- The internal resistance of the choke coil is zero; therefore, the dc voltage drop across the choke is zero.
- The loaded quality factor of the output resonant circuit is high enough so that the output current can be considered a sine wave.
- The load resistance includes parasitic resistances of the series resonant circuit; i.e., the resonant circuit is considered to be a pure reactance.
- The MOSFET ON resistance is low enough so that the current and voltage waveforms remain almost unchanged.
- The MOSFET turns on and off very fast so the transition time can be neglected. Since the transistor is turned on at zero voltage in the Class E amplifier, the turn-on transition is negligible.
- The switch duty cycle is 0.5.

Referring to Fig. 10, the current through the circuit is given by:

$$I_{dc} + I_{out}\sin(\omega t + \phi) = I_d(\omega t) + I_p(\omega t) \quad (22)$$

Where I_{dc} is the dc input current, I_{out} is the output current amplitude and $\theta = \omega t$. The current through the shunt capacitance is I_p. I_d is the current through MOSFET transistor. Figure 11 shows theoretical waveforms of the switch voltage (V_{ds}) and current (I_d).

- When the switch is ON, i.e., for $0 < \theta < \pi$,

$$V_{ds}(\omega t) = 0 \quad (23)$$
$$I_p(\omega t) = 0 \quad (24)$$

Equation 22 gives :

$$I_d(\omega t) = I_{dc} + I_{out}\sin(\omega t + \phi) \quad (25)$$

- When the switch is OFF, i.e., for $\pi < \theta < 2\pi$,

$$I_d(\omega t) = 0 \quad (26)$$

The current through the shunt capacitance is given by:

$$I_p(\omega t) = I_{dc} + I_{out}\sin(\omega t + \phi) \quad (27)$$

Hence,

$$V_{ds}(\omega t) = \frac{1}{C_d}\int I_p(\omega t)dt = \frac{1}{\omega C_d}\left[(\omega t)I_{dc} - I_{out}\cos(\omega t + \phi)\right] + K1 \quad (28)$$

$V_{ds}(\pi) = 0$, so we can obtain K1
So,

$$V_{ds}(\omega t) = \frac{1}{\omega C_d}\left[(\omega t - \pi)I_{dc} - I_{out}(\cos(\omega t + \phi) + \cos\phi)\right] \quad (29)$$

Imposing the ZVS condition given by $V_{ds}(2\pi) = 0$ then

$$\cos\phi = \frac{I_{dc}\pi}{2I_{out}} \quad (30)$$

Imposing the ZVDS $\frac{dV_{ds}(t)}{dt} = 0$
condition at the switch turn-on ($\omega t = 2\pi$)

$$I_{dc} + I_{out}\sin\phi = 0 \quad (31)$$

$$\Rightarrow \quad \sin\phi = \frac{-I_{dc}}{I_{out}} \quad (32)$$

From Eq. 30 and 32, we obtain:

$$\phi = \tan^{-1}\left(\frac{-2}{\pi}\right) = -32.48^\circ \quad (33)$$

Since the dc component of the voltage drop across the choke inductor is zero, the average value of the switch voltage is equal to the dc supply voltage. Thus:

$$V_{dd} = \frac{1}{2\pi}\int_0^{2\pi} V_{ds}(\omega t)d\omega t \quad (34)$$

Using Eq. 29, 30 and 32, we obtain:

$$V_{dd} = \frac{I_{dc}}{\pi\omega C_d} \quad (35)$$

V_{ds} is maximal when: $\frac{dV_{ds}(t)}{dt} = 0$

Then: $I_{dc} + I_{out}\sin(\omega t + \phi) = 0,\ \omega t \neq \phi$ (36)

On (32) gives $\omega t = \pi - 2\phi$ (37)

So, calculating drain source voltage:

$$V_{ds}(\pi - 2\phi) = \frac{-2\phi I_{dc}}{\omega C_d} \quad (38)$$

Using Eq. 35 and 38, one obtains:

$$\frac{V_{ds\,max}}{V_{dd}} = -2\phi\pi = 3.562 \tag{39}$$

The output impedance can be decomposed into two constituents: real and imaginary. The real part of the impedance gives a V_{dsi} voltage. The imaginary part of the impedance gives V_{dsq} voltage. The $V_{ds}(t)$ function is periodic; so we can calculate the first order coefficients of the Fourier series of this signal.

- Real part:

$$V_{dsi} = \frac{1}{\pi}\int_0^{2\pi} V_{ds}(\omega t)\sin(\omega t + \phi)d\omega t \tag{40}$$

$$V_{dsi} = \frac{-8I_{out}V_{dd}}{I_{dc}(\pi^2 + 4)} \tag{41}$$

$$R_L = \frac{V_{dsi}}{-I_{out}} = \frac{V_{dd}}{I_{dc}}\left(\frac{8}{\pi^2 + 4}\right) \tag{42}$$

- Imaginary part:

$$V_{dsq} = \frac{1}{\pi}\int_0^{2\pi} V_{ds}(\omega t)\cos(\omega t + \phi)d\omega t \tag{43}$$

$$V_{dsq} = \frac{\pi I_{out}V_{dd}}{2I_{dc}}\left(\frac{\pi^2 - 4}{\pi^2 + 4}\right) \tag{44}$$

$$X = \omega Ls = \frac{V_{dsq}}{-I_{out}} = \frac{\pi V_{dd}}{2I_{dc}}\left(\frac{\pi^2 - 4}{\pi^2 + 4}\right) \tag{45}$$

$X > 0$, then $X = \omega Ls$ with Ls is an excess inductance.
The output power is done by:

$$P_{out} = \frac{1}{2}(-I_{out})^2 R_L = \frac{1}{2}\left(\frac{I_{dc}}{\sin\phi}\right)^2 \frac{V_{dd}}{2I_{dc}}\left(\frac{8}{\pi^2 + 4}\right) \tag{46}$$

$$\text{As a result: } P_{out} = I_{dc}\ V_{dd} \tag{47}$$

$$\text{Drain efficiency is: } \frac{P_{out}}{P_{dc}} = \frac{I_{dc}V_{dd}}{I_{dc}V_{dd}} = 1 \tag{48}$$

So the class E power amplifier has a theoretical efficiency on 100%.
The quality factor of the resonant circuit is given by:

$$Q_L = \frac{\omega L}{R_L} \tag{49}$$

Using Eq. 42 and 47, the load resistance is given by:

$$R_L = \frac{8V_{dd}^2}{P_{out}(\pi^2 + 4)} \tag{50}$$

Using Eq. 45 and 47, the excess inductance is given by:

$$L_s = \frac{X}{\omega} = \frac{\pi V_{dd}^2(\pi^2 - 4)}{2\omega P_{out}(\pi^2 + 4)} \tag{51}$$

Using Eq. 49 and 50, the resonator inductor is given by:

$$L = \frac{8Q_L V_{dd}^2}{\omega P_{out}(\pi^2 + 4)} \tag{52}$$

The condition of resonance of LC circuit is $LC\omega^2 = 1$, so the expression of the resonator capacitance is given by:

$$C = \frac{P_{out}(\pi^2 + 4)}{8\omega Q_L V_{dd}^2} \tag{53}$$

The shunt capacitance is expressed from Eq. 35 and 47 by:

$$C_d = \frac{P_{out}}{\pi\omega V_{dd}^2} \tag{54}$$

Class-E simulation: To verify the theoretical results, class-E power amplifier was simulated with PSpice. We desire to achieve an output power of 150 mW. So using analytical design equations described earlier, we calculate the different class-E component values. The Table 4 contains the class-E parameter values. The theoretical value of shunt capacitor is 51.46 pF, but this value doesn't give the optimum operation; due to the assumption that C_d consists of the MOSFET output capacitance and an external linear capacitance. Using the method specified by Sokal (2001) to search the optimum operation point, one found C_d = 56.5 pF. The simulated

Table 4: Class-E parameter values

Operating frequency	13.56 MHZ
Supply voltage	V_{dd} = 3.3 V
Load resistance	R_L = 41.87 Ω
Excess inductance	L_s = 566.45 nH
Quality factor	Q_L = 10
Resonator inductor	L = 4.915 μH
Transmitter coil	$L_1 = L + L_s$ = 5.48 μH
Shunt capacitance	C_d = 56.5 pF
RF choke inductor	L_{RFC} = 12 μH
Resonator capacitance	C = 28 pF
NMOS transistor W/L	1000/0.35 (μm μm^{-1})

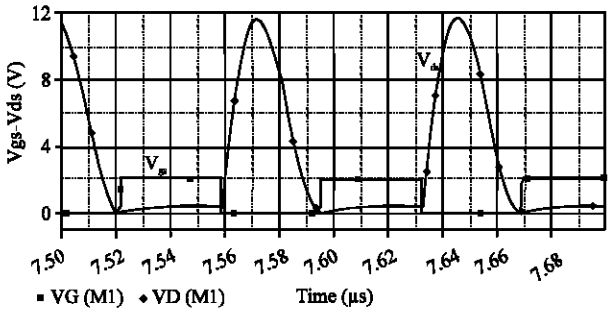

Fig. 12: Gate-Source voltage Vgs-Drsin-Source voltage Vds vs time

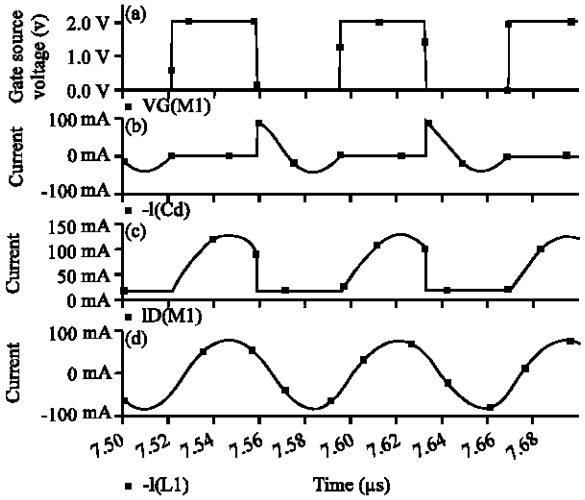

Fig. 13: Simulation waveforms, (a) Gate-Source voltage, (b) Current through the shunt capacitance, (c) Current through the NMOS transistor and (d) Current through the transmitter coil

waveforms of the gate-source voltage V_{gs} and drain-source voltage V_{ds} are shown in Fig. 12. The ZVS operation was achieved at the switching frequency 13.56 MHZ (13.56 MHZ that belongs to the ISM band: Industrial-Scientific -Medical). Using Eq. 39, we calculate the switch peak voltage V_{DSmax} = 11.75 V. The simulation value of V_{DSmax} was 11.67 V. Figure 13 shows simulation waveforms of the gate-source voltage (a), the current through the shunt capacitance (b) and current through the NMOS transistor (c). The current through the transmitter coil, Fig. 13d, is almost sinusoidal due to the high quality factor (Q_L = 10). The DC power given by the V_{dd} source (P_{DC}) is 148.2 mW, while the absorbed power by the load R_L (P_{out}) is 134 mW. The drain efficiency is then: DE = P_{out}/P_{DC} = 90.41%.

The theoretical results were validated by PSpice simulation. In particular, the switch voltage waveform satisfied both conditions for optimum operation. The drain efficiency of class-E transmitter can reach 90.4%, by Pspice simulation, using a model of a real transistor.

POWER AND DATA TRANSFER

Modulator design: In the frequency modulation or phase modulation cases, the modulated signal has a relatively wide band with compared to the amplitude modulation. Furthermore, in the implants case, the power must be transmit on an ISM band which is relatively narrow. Seen that the transmission canal in these implantable systems is the inductive link which is behaves as a selective filter, our choice approved the amplitude modulation.

The amplifier modulator structure presented in the Fig. 17, contains a pair of bipolar transistors Q_1 and Q_2 (Darlington pair). The voltage source V_2 (modulating signal) generates a binary signal with a T_{bit} = 5 µs. The NMOS transistor M_2 works as a switch. The modulation rate can be adjustable with resistance R_1. The voltage supply V_{dd} is fixed at 5V instead of 3.3V in order to recuperate the voltage drop engendered by the modulator ASK. The supply voltage of the class E power amplifier is measured between the transistor Q_1 emitter and the ground, as illustrated in the Fig. 14b. The level voltage is 2.92 V when the bit to transmit is 1 and 3.7 V in the case when the message is 0 (Fig. 14a-b). We notice that this voltage variation is around 3.3 V, the voltage for which the amplifier structure was studied. Figure 14c-d the voltage signals at the emitters and receivers coil nodes for a coupling coefficient k = 0.15. The class E power amplifier output voltage is an ASK modulated signal (Fig. 14c). We denote that the received voltage at the receiver coil nodes is also a ASK modulated signal with a modulation rate of 18.25% (Fig. 14d). The supplied power by the V_{dd} source (P_{DC}) is 274 mW. The received power, by the inductive link, consumed by the resistance R_5 is 136.6 mW, where R_5 is an equivalent resistance of all the implantable part. That gives a power efficiency of 50%.

ASK Demodulator

ASK demodulator principles: The received modulation signal, at the receiver coil, shown by the bloc diagram of the Fig. 15.

The envelope detector is consisting in a rectifier followed by a filter. The potential comparator for this application is a Schmitt's Trigger.

Design of ASK demodulator: The proposed ASK demodulator structure was based on the specific following technology: the AMS 0.35 µm, 3-metal, 2-poly, n-well standard CMOS process. Figure 17 presents all the studied inductive powering system.

The part including transistors M_3 and M_5 and the capacitor C_1 constitute the envelope detector. The transistor M_3 is set at a diode stage to realize a simple alternation rectifier. The transistor M_5 and the capacitor

C_1 provide a filter. The circuit formed by transistors M_6 to M_{13} realizes a Schmitt's Trigger. Finally, we reverse the signal formed by the two transistors M_{14} and M_{15}. The demodulated signal is presented in Fig. 16c. The voltage source V_{dd2} is in reality a regulated voltage, it is obtained from the received signal in the receiver coil nodes as a Band gap structure. The simulation results, given by the Fig. 16, have been made at a voltage source V_2 (modulating signal) which generates a binary signal with T_{bit} = 1 μs then a data rate of 1 Mbit sec^{-1}. The output signal of the envelope detector is shown in Fig. 16b.

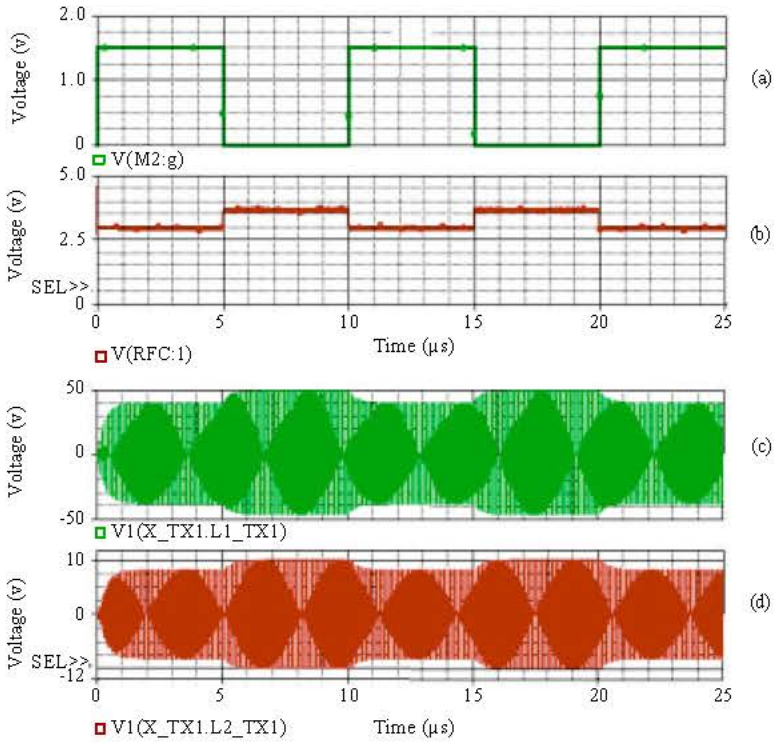

Fig. 14: (a) Binary data signal, (b) Supply voltage of the class E power amplifier, (c) Voltage signal at the transmitter coil and (d) Voltage signal at the receivers coil

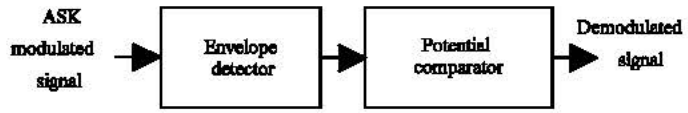

Fig.15: Block diagram of ASK demodulator

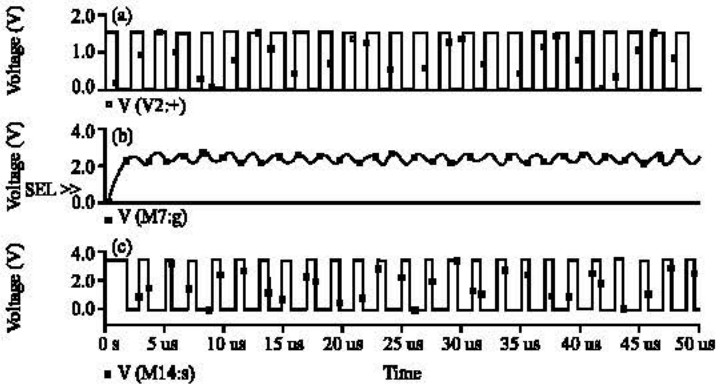

Fig. 16: (a) Binary data signal, (b) The output signal of the envelope detector and (c) Demodulated Signal

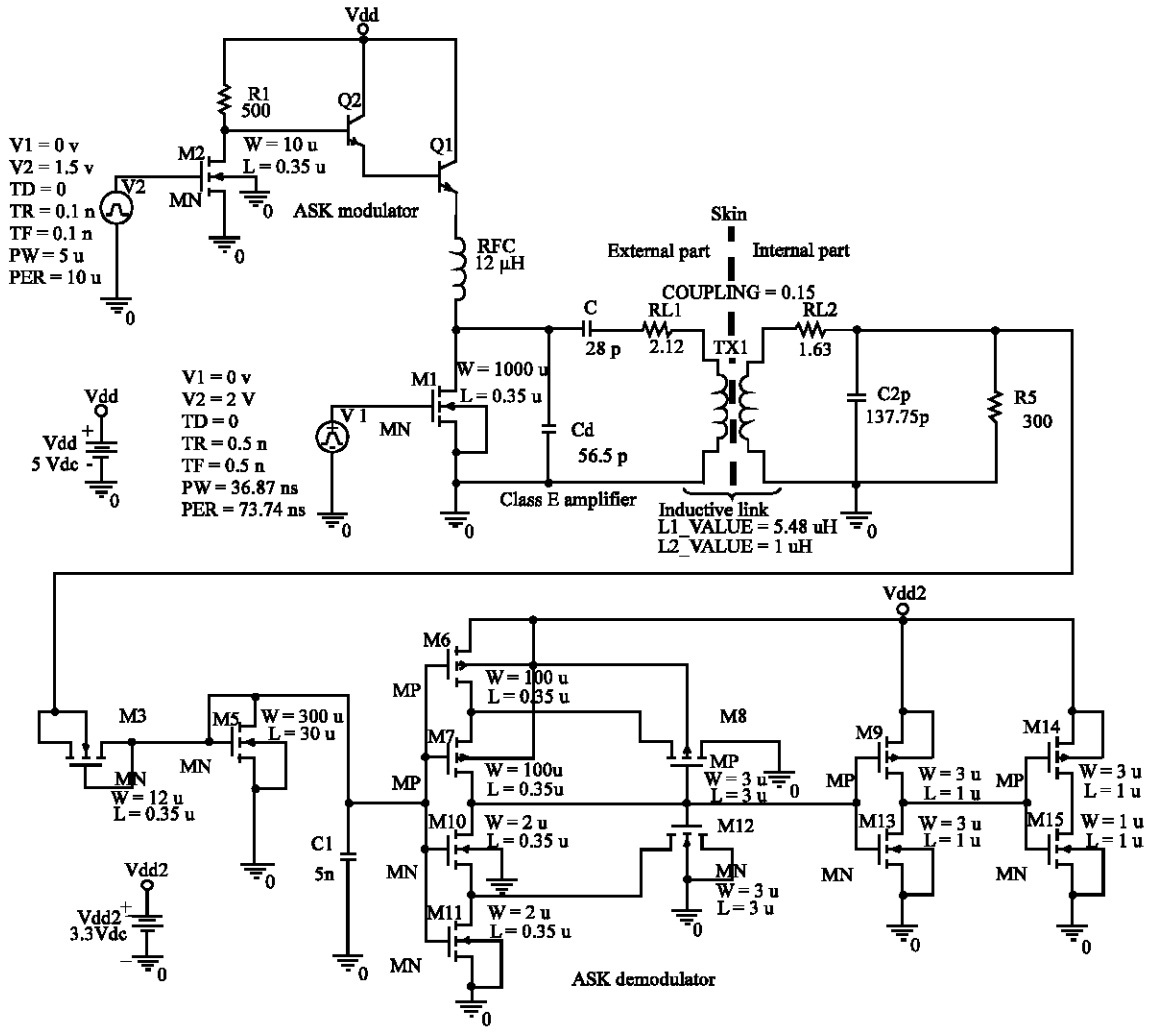

Fig. 17: Complete inductive powering system

CONCLUSION

This study presents an inductive powering system that combines power transfer with data transmission. We designed a transmitter with class E power amplifier to provide maximum power with high-efficiency. An analysis and a design of the analytical equations for a high efficiency class E amplifier were presented for optimum operation. The theoretical results were validated by PSpice simulation. The drain efficiency of class-E transmitter can reach 90.4%, by PSpice simulation, using a model of a real transistor. A power supply in the implant is equal 136 mW. Even considering some additional power loss in the DC source converters, this seems to be enough for an integrated low-power system design. This inductive powering system gives a power efficiency of 50%. The data rate transfer achieves 1 Mbit sec^{-1}. Future work will focus on the miniaturisation of the secondary circuit, resulting in an implantable ASIC.

REFERENCES

Ben Hmida, G., M. Dhieb, H. Ghariani and M. Samet, 2006. Transcutaneous power and high data rate transmission for biomedical implants. IEEE Design and Test of Integrated Systems in Nanoscale Technology (DTIS 2006), September 5-7, 2006 Tunis, Tunisia.

Burny, F., M. Donkerwolcke, F. Moulart, R. Bourgois, R. Puers and K. Van Schuylenbergh *et al*., 2000. Concept, design and fabrication of smart orthopedic implants. 2001 IPEM. Published by Elsevier Science Ltd. Medical Eng. Phys., 22: 469-479.

Catrysse, M., B. Hermans and R. Puers, 2004. An inductive power system with integrated bi-directional data-transmission. 2004. Elsevier Science B.V. Sensors and Actuators, A 115: 221-229.

Gabriel, C. and S. Gabriel, 1996. Compilation of the dielectric properties of body tissues at RF and microwave frequencies. Report AL/OE-TR-1996-0037, Armstrong Laboratory (AFMC), Radiofrequency Radiation Division, Brooks AFB, TX. http://niremf.ifac.cnr.it/tissprop/htmlclie/htmlclie.htm.

Galbraith, D.C., 1987. A wide band efficient inductive transdermal power and data link with coupling insensitive gain. IEEE Trans. Biomed. Engin., 34: 265-275.

Gervais, J.F., J. Coulombe, F. Mounnaim and M. Sawan, 2003. Bidirectional high data rate transmission interface for inductively powered devices. CCECE 2003-CCGEI 2003, Montréal, mai 2003. 0-7803-7781-8/03/© 2003 IEEE.

Ghorbel, M., M. Samet, A. Ben Hamida and J. Tomas, 2006. A 16-electrode fully integrated and versatile CMOS microstimulator dedicated to cochlear implant. J. Applied Sci., 15: 2978-2990.

Harrison, R.R. and C. Charles, 2003. A low-power low-noise CMOS amplifier for neural recording applications. IEEE J. Solid-State Circuits, 38: 958-965.

Harrison, R.R., P.T. Watkins, R. J. Kier, R.O. Lovejoy, D.J. Black, B. Greger and F. Solzbacher, 2007. A low-power integrated circuit for a wireless 100-electrode neural recording system. IEEE J. Solid-State Circuits, 42: 123-133.

Huang, Q. and M. Oberle, 1998. A 0.5-mW passive telemetry IC for biomedical applications. IEEE Trans. Solid-State Circuits, 33: 937-946.

Kazimierczuk, M.K. and K. Puczko, 1987. Exact analysis of class E tuned power amplifier at any Q and switch duty cycle. IEEE Trans. Circuits Syst., 34: 149-159.

Kendir, G.A., W. Liu, G. Wang, M. Sivaprakasam, R. Bashirullah, M.S. Humayun and J.D. Weiland, 2005. An optimal design methodology for inductive power link with class-e amplifier. IEEE Trans. Circuits Sys., I: Regular Papers, 52: 857-866.

Loeb, G.E., F.J.R. Richmond, D. Olney, T. Cameron, A.C. Dupont, K. Hood, R.A. Peck, P.R. Troyk and H. Schulman, 1998. BION/sup TM/. Bionic neurons for functional and therapeutic electrical stimulation. Proc. IEEE 20th Int. Conf. Eng. Medicine Biol. Soc., 5: 2305-2309.

Margalit, E. *et al.*, 2002. Retinal prosthesis for the blind. Elsevier science Inc. Survey of Ophthalmology, 47: 335-356.

Mohseni, P. and K. Najafi, 2005. A 1.48-mW low-phase-noise analog frequency modulator for wireless biotelemetry. IEEE Trans. Biomed. Eng., 52: 983-943.

Pamela, T.B. and K.D. Wise, 2006. A 32-Site 4-channel high-density electrode array for a cochlear prosthesis. IEEE J. Solid-State Circuits, 41: 2965-2973.

Raab, F.H., 1977. Idealized Operation of the class E tuned power amplifier. IEEE Trans. Circuits Syst., 24: 725-735.

Sawan, M., 2004. Microsystems dedicated to wireless multichannel monitoring and microstimulation: Design, test and packaging. Solid-State and Integrated Circuits Technology, 2004. Proceedings 7th International Conference, 2: 1408-1411.

Schuder, J.C., J. Gold, H.H. Stoeckle and J.A. Holland, 1976. The relationship between the electric field in a semi-infinite conductive region and the power input to a circular coil on or above the surface. Med. Biol. Eng., 14: 227-234.

Sokal, N.O. and A.D. Sokal, 1975. Class-E A new class of high efficiency tuned single-ended switching power amplifiers. IEEE J. Solid-State Circuits, 10: 168-176.

Sokal, N.O., 2001. Class-E RF Power Amplifiers. WA1HQC of Design Automation, Inc ARRL Technical Advisor. Jan/Feb 2001.

Stangel, K., S. Kolnsberg, D. Hammerschmidt, B.J. Hosticka, H.K. Trieu and W. Mokwa, 2001. A programmable intraocular CMOS pressure sensor system implant. IEEE Trans. Solid-State Circuits, 36: 1094-1100.

Suaning, G.J. and N.H. Lovell, 2001. CMOS neurostimulation asic with 100 channels, scaleable output and bidirectional radio-frequency telemetry. IEEE Trans. Biomed. Eng., 48: 248-260.

Suetsugu, T. and M.K. Kazimierczuk, 2004. Analysis and design of class e amplifier with shunt capacitance composed of nonlinear and linear capacitances. IEEE Trans. Circuits Sys., 51: 1261-1268.

Wang, C.C., Y.H. Hsueh, Y.T. Hsiao, U.F. Ghio, C.C. Huang and P.L. Liu, 2004. An implantable neural interface micro-stimulator chip with external controllability. 2004 IEEE Asia-Pacific Conference on Advanced System Integrated Circuits. Aug. 4-5, (AP-ASIC2004).

Watkins, P.T., R.J. Kier, R.O. Lovejoy, D.J. Black and R.R. Harrison, 2006. Signal amplification, detection and transmission in a wireless 100-electrode neural recording system. Proceedings 2006 IEEE Int. Symp. Circuits Systems (ISCAS).

Wise, K.D., D.J. Anderson, J.F. Hetke, D.R. Kipke and K. Najafi, 2004. Wireless implantable microsystems: High-density electronic interfaces to the nervous system. Proc. IEEE., 92: 76-97.